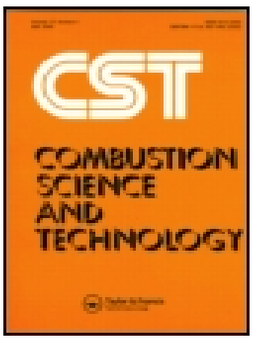

Taylor & Francis
Taylor & Francis Group

Combustion Science and Technology

ISSN: 0010-2202 (Print) 1563-521X (Online) Journal homepage: https://www.tandfonline.com/loi/gcst20

An Exploration of Advanced SLW Modeling Approaches in Comprehensive Combustion Predictions

J. Badger, B.W. Webb & V.P. Solovjov

To cite this article: J. Badger, B.W. Webb & V.P. Solovjov (2019): An Exploration of Advanced SLW Modeling Approaches in Comprehensive Combustion Predictions, Combustion Science and Technology

To link to this article: https://doi.org/10.1080/00102202.2019.1678907

Published online: 22 Oct 2019.

COMBUSTION SCIENCE AND TECHNOLOGY
https://doi.org/10.1080/00102202.2019.1678907

Taylor & Francis
Taylor & Francis Group

An Exploration of Advanced SLW Modeling Approaches in Comprehensive Combustion Predictions

J. Badger, B.W. Webb, and V.P. Solovjov

Department of Mechanical Engineering, Brigham Young University, Provo, UT, USA

ABSTRACT

Recent work demonstrated the integration of the Spectral Line Weighted-Sum-of-Gray-Gases (SLW) model for advanced modeling of gas radiation in high temperature gases in a comprehensive combustion modeling prediction scheme. This prior work compared predictions using the Reference Approach SLW model with the Domain Based Weighted-Sum-of-Gray-Gases model used in Fluent. The present work reports on the implementation of the Rank Correlated SLW model and the Locally Correlated SLW model in the combustion scenario studied in the earlier publication, complementing the Reference Approach SLW model predictions reported previously. The predictions confirm the need for such advanced radiation modeling to accurately resolve the radiative flux divergence and temperature fields, particularly in localized regions of the flame zone where very large differences in temperature and radiative heating may be found relative to the more rudimentary modeling approach. Results also reveal the dependence of the predictions for the three SLW model variants on the number of gray gases employed in the simulations. The Reference Approach and Locally Correlated SLW model predictions exhibit rather significant dependence on the number of gray gases used. It is shown that the Rank Correlated SLW model is the most robust of all models, and demonstrates that it can achieve accurate solutions with as few as 3–5 gray gases.

ARTICLE HISTORY
Received 8 February 2019
Revised 13 September 20190
Accepted 19 September 2019

KEYWORDS
Gas radiation; SLW model; rank correlated SLW model; reference approach SLW model; locally correlated SLW model

Introduction

The advanced Spectral Line Weighted-Sum-of-Gray-Gases (SLW) model is a so-called global method for simulation of radiation transfer in high temperature gases, proposed by Denison and Webb (1993). The SLW model was first developed and published for single-component, isothermal gas systems, and has been refined to treat multicomponent, nonhomogeneous, nonisothermal systems. The model has been demonstrated to produce solutions accurate to within a few percent of rigorous line-by-line benchmark predictions at a computational cost that is a tiny fraction of the cost of line-by-line predictions. A recent publication explored the implementation of the advanced SLW model for predicting radiative transfer from high temperature gases in a Fluent-based comprehensive turbulent-flow combustion prediction methodology (Webb et al. 2018). That work focused on the Reference Approach SLW method, which was the earliest formulation of the SLW model for the treatment of nonuniform (nonisothermal, nonuniform) gases based on a correlated spectrum assumption (Denison and Webb 1995a). More recent

CONTACT B.W. Webb webb@byu.edu Department of Mechanical Engineering, Brigham Young University, Provo, UT 84602

work has presented all theoretical correlated spectrum assumption variants of the SLW model in non-uniform media (Solovjov et al. 2017). Among those variants are the Rank Correlated SLW and the Locally Correlated SLW models. Whereas the Rank Correlated SLW has been shown theoretically to yield the highest overall accuracy among all correlated SLW model formulations (André et al. 2017), recent work revealed that the Locally Correlated SLW model had promise for greater accuracy in spatial regions of higher gas temperature (Solovjov et al. 2019). The present study investigates the implementation of the Reference Approach, Rank Correlated, and Locally Correlated SLW models in a comprehensive combustion prediction strategy. The combustion predictions using the various correlated SLW models are compared, and are presented with predictions employing the widely-used but more rudimentary Weighted-Sum-of-Gray-Gases (WSGG) gas radiation model in Fluent's Domain Based WSGG implementation. Further, robustness of the SLW model variants is explored by characterizing the dependence of predictions on SLW model parameters.

There has been only limited prior work in the literature reporting the use of the SLW gas radiation model in comprehensive combustion predictions. That prior work was summarized in some detail previously (Webb et al. 2018), and will not be repeated in detail here. Suffice it to say that the work of Nguen et al. (2012), Garten (2015), Rebola and Azevedo (2015), and Krishnamoorthy et al. (2010) have explored the use the SLW model in comprehensive combustion predictions. The more recent study of Darbandi et al. (2018) has added to the body of related work.

SLW modeling of radiative transfer in gases

Propagation of thermal radiation in gaseous media with spectral absorption coefficient $\kappa_\eta(\phi) = N(\phi)C_\eta(\phi)$ is characterized by the intensity of radiation $I_\eta(s, \mathbf{\Omega})$ at wavenumber η along a path s in a direction $\mathbf{\Omega}$. Here, $C_\eta(\phi)$ is the local spectral absorption cross-section, and $N(\phi)$ is the molar density at the local gas thermodynamic state, symbolically represented by the composite vector $\phi = \{T, p, Y_i\}$ which denotes dependence on temperature T, total pressure p, and species mole fractions Y_i. The detailed continuous gas absorption cross-section $C_\eta(\phi)$ can include millions of spectral vibration-rotation lines with complex dependence on the local thermodynamic state. The SLW spectral model replaces the absorption cross-section by a piece-wise constant histogram spectrum represented as $C_\eta(\phi) = C_j$ in the spectral regions $\eta \in \Delta_j$, where $\Delta_j = \left\{\eta : \tilde{C}_{j-1} < C_\eta(\phi) < \tilde{C}_j\right\}$ are the gray gas spectral intervals defined by supplemental cross-sections $\tilde{C}_j$, $j = 0, 1, 2, \ldots, n$, where n is the number of gray gases in the model, C_j are the gray gas absorption cross-sections, and a_j are the corresponding weights describing the contribution of each gray gas to the total radiative transfer. The weights a_j are calculated using the Absorption Line Blackbody Distribution Function (ALBDF) (Denison and Webb 1995a; Solovjov, Webb, André 2018). Integrating the spectral RTE over spectral intervals Δ_j (provided that these intervals are maintained the same for all spatial locations s) yields the gray gas RTEs (Solovjov et al. 2016)

$$\partial I_j(s, \mathbf{\Omega})/\partial s = -\kappa_j(s) I_j(s, \mathbf{\Omega}) + a_j(s)\kappa_j(s) I_b[T(s)] \tag{1}$$

The ALBDF $F(C,\phi,T_b)$ as a function of continuous variable C is defined as the fraction of the total blackbody emissive power $E_b(T_b)=\sigma T_b^4$ emitted at source temperature T_b that lies in the part of the spectrum where $C_\eta(\phi)$ is below a prescribed value C (Denison and Webb 1993, 1995). The ALBDF is a strictly increasing function of the variable C and is therefore invertible, with the inverse ALBDF expressed as a function of the continuous F-variable as $C=C(F,\phi,T_b)$. The ALBDF has been calculated from the detailed absorption cross-section for a range of temperatures, partial pressures (where appropriate), and total pressures for H_2O, CO_2, and CO using spectral absorption cross-sections generated using parameters drawn from the HITEMP 2010 spectroscopic database, and has been tabulated as a function of dependent variables by Pearson et al. (2014).

In non-isothermal/non-homogeneous gas media the thermodynamic state $\phi(s)$ varies with location s. To avoid appearance of additional so-called Leibnitz terms of integration of the RTE over the spectrum, the spectral intervals of integration $\Delta_j=\left\{\eta:\tilde{C}_{j-1}<C_\eta(\phi(s))<\tilde{C}_j\right\}$ must be maintained the same for all spatial locations s. These additional Leibnitz terms can be ignored, incurring error in the radiative transfer predictions. Alternatively, the Leibnitz terms can be eliminated by maintaining the spectral intervals Δ_j constant at all locations by invoking a correlated SLW model assumption (Denison and Webb 1995a; Solovjov et al. 2016).

The assumption of a rank correlated spectrum applied to the SLW model is formulated as follows (André et al. 2017; Solovjov et al. 2017). For any set of gray gas supplemental absorption cross-sections $\tilde{C}_j^1$ prescribed at a location for gas thermodynamic state ϕ_1, there exists a set of cross-sections $\tilde{C}_j^2$ such that

$$\left\{\eta:C_\eta(\phi_1)<\tilde{C}_j^1\right\}=\left\{\eta:C_\eta(\phi_2)<\tilde{C}_j^2\right\}=\tilde{\Delta}_j \tag{2}$$

The spectral intervals defined by the cross-sections $\tilde{C}_j^2$ at state 2 and those defined by $\tilde{C}_j^1$ at state 1 are the same. These wavenumber intervals are denoted $\tilde{\Delta}_j$. Therefore, the equality

$$F\left(\tilde{C}_j^1,\phi_1,T_b\right)=F\left(\tilde{C}_j^2,\phi_2,T_b\right)\ \text{ for }\ j=1,2,3,....,n \tag{3}$$

relating the ALBDF of the rank correlated gray gas supplemental absorption cross-sections $\tilde{C}_j^1$ and $\tilde{C}_j^2$ at any two arbitrary thermodynamic states ϕ_1 and ϕ_2 is always satisfied when the same blackbody source temperature T_b is prescribed for both sides of Equation (3). This provides the same fraction of the total blackbody emissive power $E_b(T_b)$ at source temperature T_b in the same spectral intervals $\tilde{\Delta}_j$ at the two thermodynamic states. The implicit Equation (3) relates the supplemental absorption cross-sections which preserve the gray gas wavenumber intervals at different thermodynamic states. Different SLW approaches vary by the choice of the gray gas supplemental cross-sections $\tilde{C}_j$ and the blackbody source temperature T_b used in Equation (3), and were first outlined theoretically by Solovjov et al. (2017). They are distinguished by the manner in which the blackbody source temperature T_b in Equation (3) is specified, and by the different approaches for determining the local gray gas absorption cross-sections. SLW methods for which T_b is fixed at all locations in the medium are the original Reference Approach SLW (RA-SLW) model and the Rank Correlated SLW (RC-SLW) model, presented and explored in detail elsewhere (Denison and Webb 1995a; Solovjov et al. 2017). Those for which the blackbody

source temperature is the local gas temperature $T_b = T_{loc}$ are termed "locally correlated" models. Recently the Locally Correlated SLW (LC-SLW) model was presented and investigated in detail by Solovjov et al. (2019), and compared to other SLW model variants. It should be noted that Equations (2) and (3), which are used for construction of the correlated SLW models, are exactly valid for rigorously correlated (or, more rigorously, comonotonic) gas spectra. In this case, the conservation of the spectral intervals for different thermodynamic states is rigorously preserved and the relations are exact. However, real gas spectra are not perfectly correlated, and therefore, the local cross-sections constructed using Equation (3) may not generate the same spectral intervals Δ_j at different gas thermodynamic states. Thus, all reference approaches are approximations for real gas spectra. Because of this, the different correlated SLW versions can perform differently.

Outline of correlated SLW approaches

Construction of the local spectral model in the SLW method consists in finding the local values of the gray gas absorption coefficients and their weights in the gray gas RTE, Equation (1):

$$\kappa_j^{loc} = \kappa_j(s),\ a_j^{loc} = a_j(s) \tag{4}$$

The following notation in outline of the SLW approaches is used for the local parameters

$$\phi_{loc} = \phi(s) = \left\{T_{loc} = T(s), p_{loc} = p(s), Y_{i,loc} = Y_{i,loc}(s)\right\} \tag{5}$$

and for the arbitrarily chosen reference parameters $\phi_{ref} = \left\{T_{ref}, p_{ref}, Y_{i,ref}\right\}$. Also, N^{loc} is the local gas molar density and Y^{loc} is the local gas specie mole fraction.

Division of the gray gases in the RA-SLW and LC-SLW methods consists of partitioning the C-variable into logarithmically evenly spaced supplemental absorption cross-sections, $\tilde{C}_j^{ref} = C_{\min}(C_{\max}/C_{\min})^{j/n}$, j = 0,1,2, …, n and absorption cross-sections $C_j^{ref} = (\tilde{C}_{j-1}^{ref}\,\tilde{C}_j^{ref})^{1/2}$, where $C_{\min}$ and $C_{\max}$ are chosen to effectively cover the entire absorption spectrum. Division of the gray gases for the RC-SLW method is performed by partitioning of the F-variable into supplemental values $0 \le \tilde{F}_j^{ref} \le 1$ and F_j^{ref} for $\tilde{F}_{j-1}^{ref} < F_j^{ref} < \tilde{F}_j^{ref}$, where Gauss-Legendre quadratures are used to define the subdivision.

The methodology for determining the local gray gas absorption coefficients (absorption cross-sections) and associated gray gas weights needed for the solution of the gray gas RTE Equation (1) is outlined for each of the SLW models below.

Reference approach SLW (RA-SLW) model

The Reference Approach SLW model was first proposed by Denison and Webb (1995) as follows:

(1) The reference values of the F-variable are calculated using the direct ALBDF:

$$\tilde{F}_j^{ref} = F\left(\tilde{C}_j^{ref}, \phi_{ref}, T_{ref}\right) \tag{6}$$

(2) The local values of the supplemental absorption cross-sections and the local gray gas absorption coefficients are calculated using the inverse ALBDF:

$$\tilde{C}_j^{loc} = C\left(\tilde{F}_j^{ref}, \phi_{loc}, T_{ref}\right),\ \kappa_j^{loc} = N^{loc} Y^{loc} \left(\tilde{C}_{j-1}^{loc} \tilde{C}_j^{loc}\right)^{1/2} \tag{7}$$

(3) The local gray gas weights are calculated using the ALBDF:

$$a_j^{loc} = F\left(\tilde{C}_j^{ref}, \phi_{ref}, T_{loc}\right) - F\left(\tilde{C}_{j-1}^{ref}, \phi_{ref}, T_{loc}\right) \tag{8}$$

Locally correlated SLW (LC-SLW) model

The Locally Correlated SLW model proceeds with the following steps (Solovjov et al. 2017, 2019):

(1) The local values of the *F*-variable and the local gray gas weights are calculated using the ALBDF:

$$\tilde{F}_j^{loc} = F\left(\tilde{C}_j^{ref}, \phi_{ref}, T_{loc}\right),\ F_j^{loc} = F\left(C_j^{ref}, \phi_{ref}, T_{loc}\right),\ a_j^{loc} = \tilde{F}_j^{loc} - \tilde{F}_{j-1}^{loc} \tag{9}$$

(2) The local values of the absorption cross-sections and the local gray gas absorption coefficients are calculated using the inverse ALBDF:

$$C_j^{loc} = C\left(F_j^{loc}, \phi_{loc}, T_{loc}\right),\ \kappa_j^{loc} = N^{loc} Y^{loc} C_j^{loc} \tag{10}$$

Rank correlated SLW (RC-SLW) model

In the Rank Correlated SLW model the reference blackbody source temperature T_b must first be chosen (the spatial average is used in this paper) (André et al. 2017; Solovjov et al. 2017). Then the spectral model is constructed by the following two steps:

(1) The local values of the supplemental absorption cross-sections and the local gray gas absorption coefficients are calculated using the inverse ALBDF:

$$\tilde{C}_j^{loc} = C\left(\tilde{F}_j^{ref}, \phi_{loc}, T_b\right),\ C_j^{loc} = C\left(F_j^{ref}, \phi_{loc}, T_b\right),\ \kappa_j^{loc} = N^{loc} Y^{loc} C_j^{loc} \tag{11}$$

(2) The local gray gas weights are then calculated using the ALBDF:

$$a_j^{loc} = F\left(\tilde{C}_j^{loc}, \phi_{loc}, T_{loc}\right) - F\left(\tilde{C}_{j-1}^{loc}, \phi_{loc}, T_{loc}\right) \tag{12}$$

The principal difference between the SLW methods outlined above may be summarized as follows. The RA-SLW method applies the reference condition for the gas state ϕ_{ref} and for

the blackbody source temperature $T_b = T_{ref}$. The RC-SLW method avoids specification of the gas reference state ϕ_{ref} (while still specifying T_b), whereas the LC-SLW method avoids application of the reference value of the blackbody source temperature T_b (while still specifying T_{ref}). Practically, the greater the number of gray gases used in the prediction the higher the accuracy. Prior work has demonstrated theoretically that the RC-SLW model is the optimal correlated SLW model (André et al. 2017), and produces the greatest overall accuracy. Additional study has revealed, however, that the LC-SLW model may yield improved predictions in regions of high gas temperature (Solovjov et al. 2019).

Because the WSGG model has been in use for prediction of radiation transfer in gases for a number of years, it bears brief description here. The classical WSGG model is formulated as the solution of multiple RTEs for fictitious "gray gases" and a fictitious "clear gas" to simulate the radiation heat transfer behavior of combustion gas mixtures. The total radiation intensity is then the summation of radiation intensity for all gray gases. In the classical WSGG model the local gray gas absorption coefficients and their weights appearing in Equation (1) are calculated through empirical fits of gas total emissivity data. Several sets of coefficients for the classical WSGG method have been developed, and are found in the literature. Because of the nature of the WSGG model formulation, WSGG coefficients are derived for specific H_2O – CO_2 partial pressures and pressure ratios corresponding to complete combustion of different hydrocarbon fuels under one atmospheric pressure (Webb et al. 2018).

Problem statement

The same case studied previously (Webb et al. 2018) is used as the testbed for exploring the prediction characteristics of the different SLW gas property models outlined here. That case is the work of Andersson et al. (2008) reporting oxy-combustion experiments using propane as the fuel. Oxy-combustion is a scenario where accurately treating the contribution of radiative heat transfer is particularly important due to very high concentrations of radiatively participating CO_2. In the problem studied flue gas was cooled, dried, and reinjected into the furnace as the diluent for the oxygen in place of the nitrogen that was present in air-fired flames. The furnace studied was cylindrical, with a diameter of 0.8 m and length of 2.4 m, fired downward. Three sets of experimental data were reported by Andersson *et al.*, but two of the experimental conditions reportedly yielded very luminous flames and therefore, radiative transfer in these cases was strongly influenced by the presence of soot. The remaining case was only slightly luminous, and the radiative transfer was thus influenced by soot to a much lesser extent. It is for this latter case that predictions have been made here. The contribution to radiative transfer from soot is assumed to be weak for the case simulated, and is neglected in this study.

The propane burner used in the experiments as described by Andersson et al. (2008) and summarized by Webb et al. (2018) featured a fuel lance (diameter = 34 mm) and two cylindrical feed-gas registers. The primary register was swirled with a fin angle of 45 deg and featured an outer diameter of 52 mm. The secondary register was swirled with a fin angle of 15 deg and had an outer diameter of 92 mm. For the case simulated here the recycled flue gas was 21% oxygen (by volume) when it was injected into the burner at 300 K. The flow rate for the primary oxidant register was 37 m^3/h at standard conditions and for the second register was 54 m^3/h at standard conditions. Enough fuel was injected to reach a stoichiometric ratio of 1.15. The walls of the

furnace were refractory-lined, and four cooling tubes of unknown dimensions and temperatures were inserted axially along the walls and equally spaced circumferentially in the furnace, to cool the flame. Wall temperature and emissivity were not reported in the study. Consequently, the effective wall temperature from these two effects was assumed arbitrarily to be 873 K with gray emissivity of 0.8.

The commercial CFD code Fluent was used to solve numerically the governing equations. Fluent uses the control volume method (Patankar 1980) on unstructured grids to solve numerically the governing conservation equations. For the sake of simplicity, an axisymmetric Fluent simulation model was constructed using the conditions described above. The swirl was included by imposing axial and tangential components of the inlets near the fin angles described in the paper. The mass flow inlets for both fuel and oxidizer were set to 300 K with flow rates as described above. The flow field was assumed to be turbulent and the standard k – ε model was used to model the turbulence. The chemical reaction was modeled using a simple two-step propane combustion model:

$$C_3H_8 + 3.5O_2 \rightarrow 3CO + 4H_2O \text{ and } CO + 0.5O_2 \rightarrow CO_2$$

The eddy dissipation model was used for turbulence-chemistry interaction.

The SLW gas radiation model is capable of handling all principal combustion gas species, H_2O, CO_2, and CO, and empirical correlations for the ALBDF, or tabulated ALBDF data are available for all three species (Pearson et al. 2014). In this study, all three species were included in the radiative transfer calculations, using locally calculated concentrations of H_2O, CO_2, and CO at each iteration to predict the radiative transfer. It is possible to easily include the influence of nonscattering soot in the SLW model as well by treating it as a pseudo-gas and generating an equivalent ALBDF for inclusion in the gas mixture as described and demonstrated by Solovjov and Webb (2001). However, as was stated previously, a nonluminous combustion case was simulated here and consequently, soot was not included in the prediction.

The default model for determining the radiative properties of gases in Fluent is the Domain Based WSGG model. Fluent has built-in coefficients for the 4-RTE WSGG formulations. They are taken from Smith et al. (1982) and Coppalle and Vervisch (1983). The coefficients from Smith *et al.* were calculated for $p_{CO_2} = 0$ (partial pressure of CO_2), $p_{H_2O} = 0$ (partial pressure of water vapor), $p_{H_2O} = 1$ atm, for discrete values of the partial pressure ratios $p_{H_2O}/p_{CO_2} = 1$ and $p_{H_2O}/p_{CO_2} = 2$. These data are valid for $p = p_{H_2O} + p_{CO_2} = 1$ atm (total pressure), and temperatures between 600 K and 2400 K. The coefficients of Coppalle and Vervisch used by Fluent have been developed, again for discrete values of the partial pressure ratios $p_{H_2O}/p_{CO_2} = 1$ and $p_{H_2O}/p_{CO_2} = 2$, with valid temperature range between 2500 K and 3000 K. Based on the temperature and species partial pressures in the mixture Fluent chooses the closest data. Between 2400 K and 2500 K, Fluent interpolates the two sets of data linearly with temperature. For total pressure p other than 1 atm Fluent uses scaling rules from Edwards and Matavosian (1984), which presents scaling data for total pressure of 0.1 atm, 0.3 atm, 3 atm, and 10 atm at temperatures of 800 K, 1200 K, 1600 K, and 2000 K. The WSGG model is not configured to include CO in the radiative transfer predictions, and its influence was therefore neglected in the WSGG simulations of this study.

Instead of solving four RTEs as formulated by the original WSGG formulation, Fluent's Domain Based WSGG model seeks to economize computationally by solving

only one RTE to reduce the computational effort. This is done by using the WSGG coefficients to calculate the gas mixture total emissivity ε. Once the gas total emissivity is obtained, a single gray gas mixture absorption coefficient to be used in the RTE solution is calculated using the relation $\kappa = -(1/L_e)\ln(1-\varepsilon)$ where $L_e = 3.6V_{tot}/A_{tot}$ and V_{tot} is the total volume and A_{tot} is the total surface area of the simulation domain.

Fluent allows users to solve multiple RTEs via a User Defined Function (UDF) and provides macros for the implementation. The SLW model by itself is very flexible and can be arranged readily to solve an arbitrary number of RTEs using Fluent's framework. The three variants of the SLW model (RA-SLW, LC-SLW, and RC-SLW models) as described in the foregoing sections were implemented using Fluent's User Defined Functions. Tabulated ALBDF data (Pearson et al. 2014) were used in all SLW model simulations. The multiplication method was applied in the SLW methods to treat the mixture of gas species (Denison and Webb 1995b).

A grid refinement study was undertaken to determine the appropriate spatial and angular grid to produce grid-independent solutions. The outcome of that study yielded the predictions reported here, employing 67,611 high-quality quad mesh cells with clustering in the flame region. Fluent provides several RTE solution methods, and the finite volume variant of the Discrete Ordinates (DO) model was used here. Systematic refinement of the angular grid employed in the DO radiation model resulted in the adoption of 4 divisions in the θ and ϕ directions, 2 pixels in θ and ϕ, which was a compromise between accuracy and computational effort. The RTE was solved with the other conservation equations at each iteration in this study.

To provide comparison, simulations were performed on the same grid with the RA-SLW, LC-SLW, and RC-SLW gas radiation models, as well as the Fluent Domain Based WSGG model. Further, the influence of the number of gray gases used in the SLW model was explored by performing simulations with n = 10, 5, and 3 gray gases for each of the RA-SLW, LC-SLW, and RC-SLW models.

This work will focus on the predicted gas temperature and radiative heating distributions for the gas spectral property models explored. The radiative heating Q is defined as the local radiative source in the energy equation, $Q = -div(\vec{q}_{rad})$, where $\vec{q}_{rad}$ is the local total (spectrally-integrated) radiative flux vector.

Results and discussion

Figure 1 illustrate contours of the predicted temperature (left) and radiative heating (right) for the four gas spectral property models considered here (Domain Based WSGG, RA-SLW, RC-SLW, and LC-SLW models). Only the flame region (1.75 m of furnace length nearest the burner) is shown in the figure. The upper half of each of the six panels illustrates the predictions for the WSGG, LC-SLW, or RC-SLW model, and the lower half shows for comparison the corresponding prediction for the earliest correlated SLW approach for the treatment of nonuniform media, the RA-SLW model. All SLW model predictions shown in this figure employed 10 gray gases. Figure 1 reveals that all predictions are qualitatively similar, featuring ignition, a cool curtain due to the introduction of primary and secondary oxidant in the cylindrical registers, a reacting core, and highest temperatures in a cylindrical region near the edge of the reaction zone. Only modest differences in predicted temperatures are observed among the three SLW model

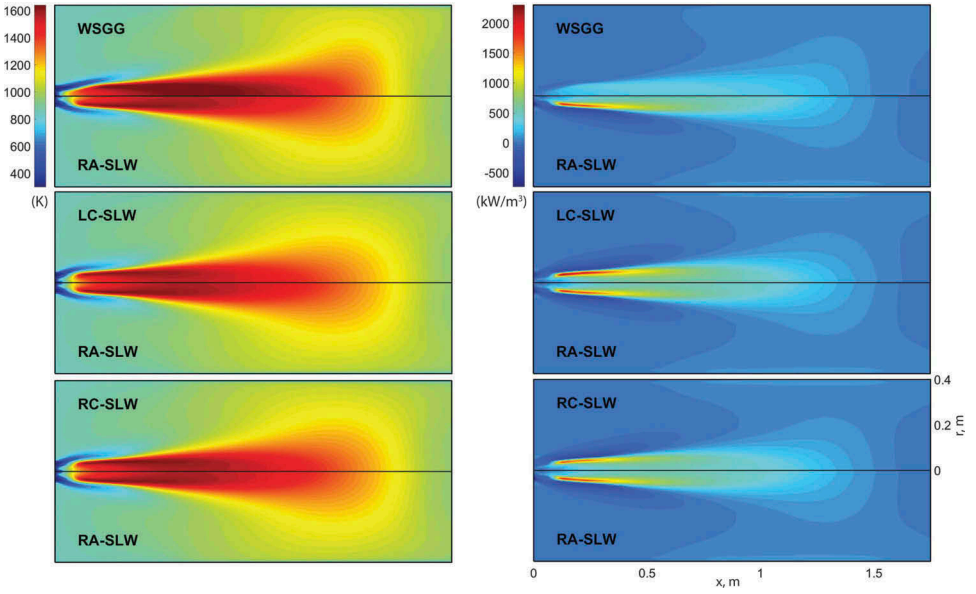

Figure 1. Contours of temperature, K (left) and radiative heating, kW/m^3 (right) for the WSGG and three SLW models. Only the flame zone (1.75 m length) is shown.

variants. However as seen in the upper panel (left) the WSGG model yields a significantly different shape of the flame zone, with a somewhat flared and blunt flame tip compared to SLW model predictions. Further, there is a substantially larger region of high gas temperature in the flame zone for the WSGG model. It is also seen that the WSGG model predicts earlier ignition and a more conical flame region near the burner than the SLW models. The local radiative heating contours of Figure 1 (right) show again that the predictions for the three SLW model variants are qualitatively similar. However, the SLW models exhibit a localized region of significantly higher radiative heating on the edge of the flame than predicted by the WSGG model. Thus, while all three SLW models produce similar temperature and radiative heating distributions, the predictions differ significantly from those of the more rudimentary WSGG model. These differences in WSGG predictions are observed primarily in (i) the narrowed shape of the flame near the inlet, (ii) the size of the high-temperature region in the flame core, and (iii) the blunted shape of the flame downstream of the high temperature reaction zone.

To highlight differences between predictions for the various models, Figure 2 shows disparity contours for the WSGG, LC-SLW, and RC-SLW model relative to the RA-SLW model predictions. The local disparity shown is the local difference between a particular model prediction of gas temperature or radiative heating and the corresponding local prediction for the RA-SLW model. For example, the upper left panel shows contours of predicted temperatures for the WSGG model minus the prediction from the RA-SLW model. This highlights the quantitative differences in predictions among the various gas spectral property models employed.

The temperature disparity map of Figure 2 (left) reveal that the WSGG predictions are as much as 400-500 K lower at the edge of the flame zone, and higher (by perhaps 400-500

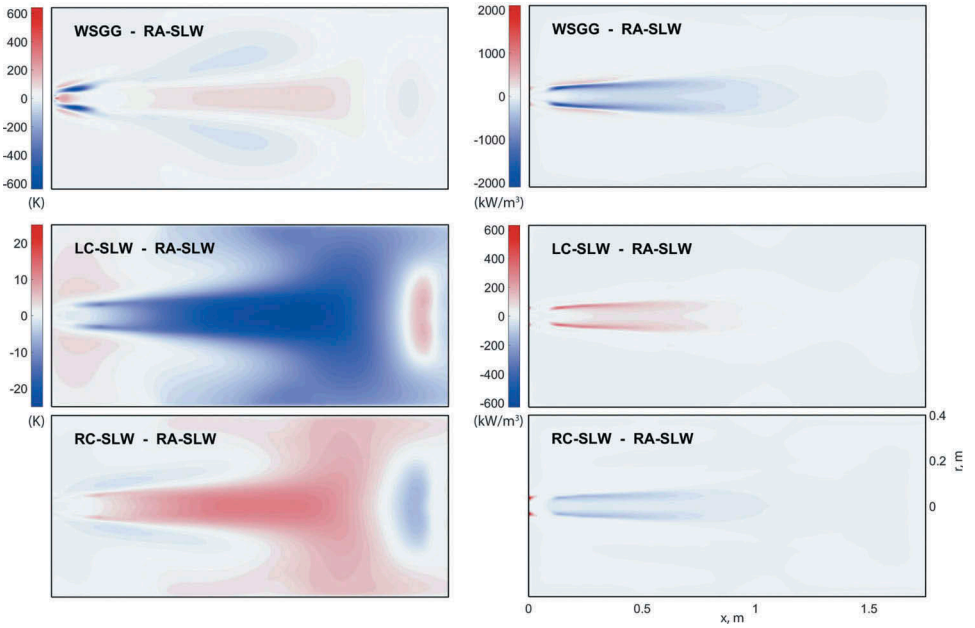

Figure 2. Disparity contours for temperature (left) and radiative heating (right) comparing the WSGG, LC-SLW, and RC-SLW models relative to the RA-SLW method.

K) near the burner exit than the RA-SLW model. The conical cold zone near the burner observed in the temperature contours of Figure 1 for the WSGG model is also seen clearly in Figure 2. The LC-SLW model yields predictions of local temperature quantitatively similar to the RA-SLW model early in the flame, with modestly lower temperatures (15–20 deg K) later. (Note the change of scale in the lower two panels of Figure 2.) Finally, RC-SLW model predictions for temperature (in the lower left panel, using the same scale as the LC-SLW model prediction disparity map) are nearly identical to those of the RA-SLW model early in the flame zone, and modestly higher (5–10 deg K) in the flame core downstream.

The radiative heating disparity maps of Figure 2 (right) illustrate that the WSGG model predictions are dramatically lower than the RA-SLW model by as much as 1000 kW/m^3 in the thin cylindrical region at the edge of the flame. The predicted radiative heating for the LC-SLW model is higher at the edge of the flame by about 300 kW/m^3. The lower right panel suggests that differences in predictions of radiative heating for the RC-SLW and RA-SLW models arerather modest, near 150 kW/m^3 in the cylindrical reaction zone and much lower elsewhere in the furnace.

The approximate 400-500 K difference in temperature observed in the top panels of Figure 2 between the WSGG and RA-SLW models is largely due to the difference in predicted flame shape near the inlet. Figure 3 shows predicted radial profiles of temperature and radiative heating in the flame zone at a furnace axial location of x = 0.1 m from the burner. These profiles illustrate quite clearly the predicted differences in the shape of the reaction zone and correspondingly higher maximum

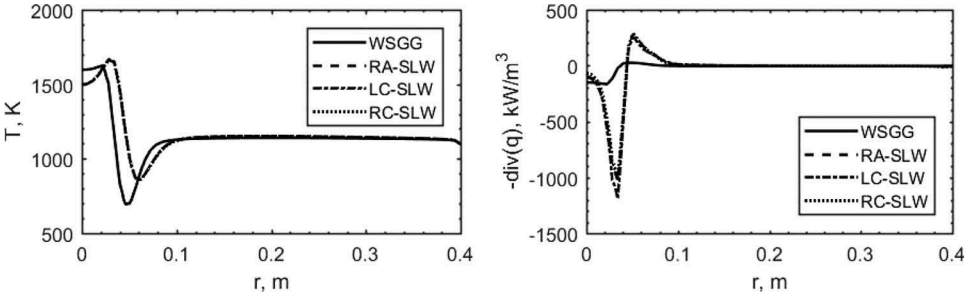

Figure 3. Radial profiles of temperature (left) and radiative heating (right) at x = 0.1 m.

temperatures and lower flame-core temperature near the burner predicted by the SLW models relative to the WSGG model. Indeed, one may conclude that to accurately resolve ignition and flame zone shape and corresponding temperature and radiative heating one much adopt more sophisticated property models for the radiation transfer in the gases.

Differences in predicted gas temperature and local radiative heating among the three correlated SLW models may be further explored. Figure 2 reveals that the LC-SLW model predicts temperatures in the flame region nearly 25 K lower than that predicted by the RA-SLW model, while the RC-SLW model predicts temperatures around 15 K higher than the RA-SLW model. These observations may be quantified from differences in temperature and radiative heating displayed in Figure 2 as the normalized Average Difference and Maximum Difference in predictions, calculated from local temperature T and local radiative heating $Q = -div(\vec{q}_{rad})$ distributions as follows

$$Avg\ Diff = \frac{\int_V |T - T_{ref}|dV \Big/ V_{tot}}{\int_V T_{ref}\, dV \Big/ V_{tot}} \quad \text{and} \quad Max\ Diff = \frac{\max(|T - T_{ref}|)}{\int_V T_{ref}\, dV \Big/ V_{tot}} \tag{13}$$

$$Avg\ Diff = \frac{\int_V |Q - Q_{ref}|dV \Big/ V_{tot}}{\max(|Q_{ref}|)} \quad \text{and} \quad Max\ Diff = \frac{\max(|Q - Q_{ref}|)}{\max(|Q_{ref}|)} \tag{14}$$

Here, the subscript "*ref*" refers to the reference simulation against which the normalized Average Difference and Maximum Difference are compared in the calculation. It may be mentioned that while other arbitrary normalizations may be proposed, the simple metrics chosen here are sufficient to illustrate the aggregate differences in predictions among the various models.

Table 1 lists the normalized Average and Maximum Difference in temperature and radiative heating for the WSGG, LC-SLW, and RC-SLW model predictions relative to the RA-SLW model. The table reveals, as observed graphically in Figure 2, that the WSGG model yields large Average and Maximum Differences relative to the RA-SLW model. By

Table 1. Normalized average difference and maximum difference in predicted temperature and radiative heating relative to the RA-SLW model.

	Temp. Diff.*		Rad. Heat. Diff.*	
Method	Max	Avg	Max	Avg
WSGG	63.9%	1.8%	92.8%	0.36%
LC-SLW	2.5%	0.5%	19.6%	0.05%
RC-SLW	1.2%	0.2%	35.0%	0.11%

*Relative to RA-SLW model.

contrast, the Maximum and Average Differences between LC-SLW and RC-SLW models and the corresponding RA-SLW model predictions are much smaller. Note that while Figures 1–3 reveal that the WSGG model prediction differs significantly from the SLW models in the flame region, Table 1 suggests that the Average Differences in temperature and radiative heating relative to the RA-SLW predictions are quite modest, 1.8% and 0.36%, respectively. It would seem that while the rudimentary WSGG gas radiation property model fails to accurately resolve local phenomena in the flame zone, its overall predictions are not unreasonably inacccurate relative to the predictions of the more sophisticated SLW models. Further, it may be noted that while the magnitudes of the Average Difference are due in large part to the choice of normalization, the cylindrical geometry of the furnace also plays a factor, weighting the values near the wall higher than those near the core of the flame where differences are most prominent.

To investigate the robustness of each of the predictions employing the SLW model formulations, the number of gray gases n used in all methods was varied, with predictions carried out for n = 10, 5, and 3. While a higher number of gray gases used in the SLW model simulation yields greater accuracy, there is an attendant increase in computation time, as will be discussed later. Thus, it is desirable to understand how the predictions vary with the number of gray gases used, and more practically, how few gray gases may be employed and still achieve accurate results. The outcome of these simulations are illustrated in Figure 4, where the number of gray gases used in each model is denoted by the subscript for each of the SLW model variants. The upper half of each panel illustrates contours of temperature or radiative heating for a simulation using n gray gases (3 or 5), and the lower half of each panel shows the corresponding prediction for the presumably more accurate 10-gray-gas simulation using the same SLW model. Thus, one can compare the difference in predictions as n is reduced.

The temperature contour data of Figure 4 (left panels) reveal only modest differences in temperature between the n = 5 predictions and the n = 10 predictions for the RA-SLW, LC-SLW, and RC-SLW models. Reducing the number of gray gases to n = 3, however, yields considerable differences compared to the n = 10 simulation. In the 3-gray-gas results the RA-SLW and LC-SLW models predict more flared and blunt flame zones, with a larger region of localized higher gas temperature at the edge of the flame. Indeed, one may see that the flame zone is both longer and wider for the RA-SLW and LC-SLW models as the number of gray gases is reduced. By contrast, the Rank Correlated SLW model temperature prediction for n = 3 and n = 10 are quantitatively very similar, exhibiting only modest dependence on the number of gray gases. The radiative heating contours in Figure 4 (right panels) show corresponding trends in model prediction dependence on n. The localized

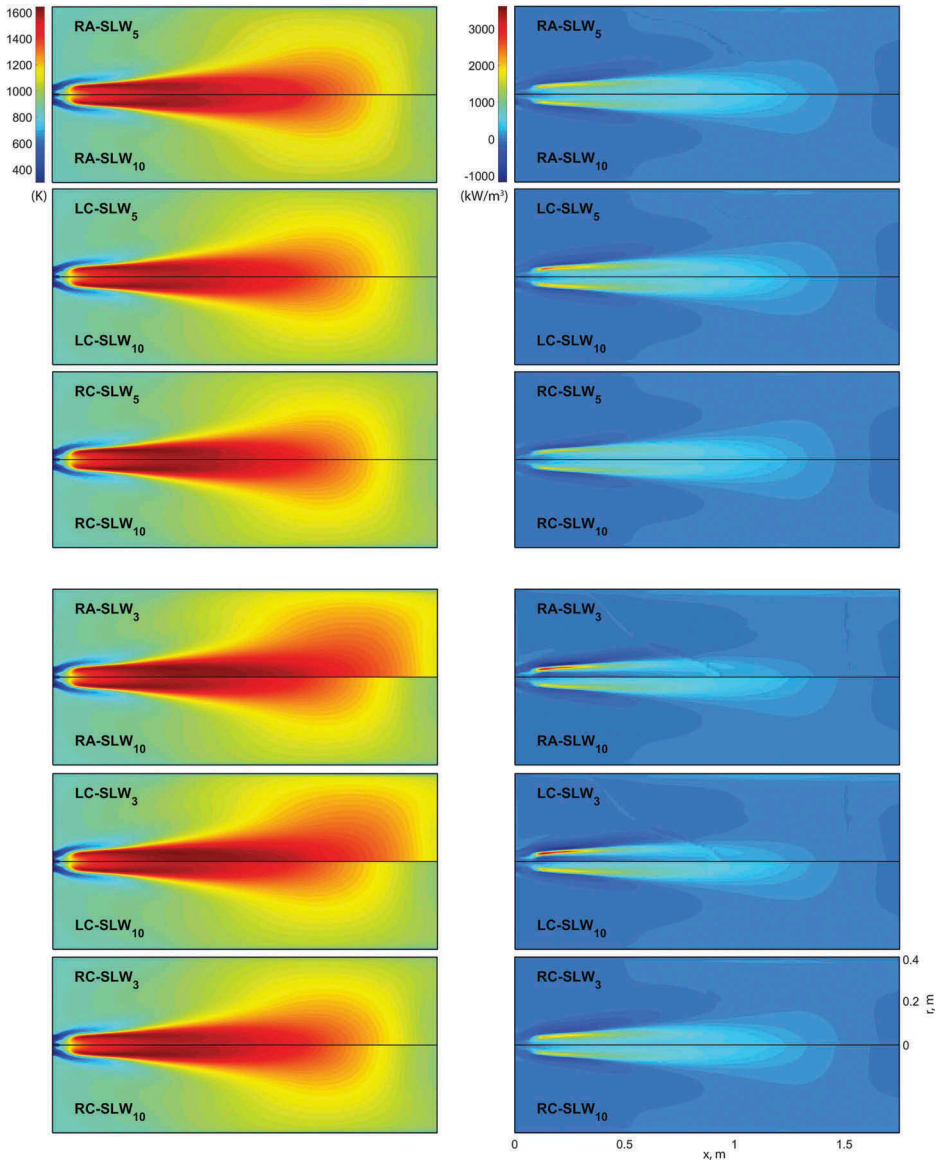

Figure 4. Contours of predicted temperature (left) and radiative heating (right) for n = 3, 5, and 10 gray gases. The lower half of each panel shows the 10-gray-gas case.

region of high radiative heating at the edge of the flame zone reveals higher values of Q as the number of gray gases is reduced for the RA-SLW and LC-SLW models. The RC-SLW model, however, exhibits very little difference in the radiative heating contours as n is reduced from 10 to 5, and further from 5 to 3.

The differences observed in Figure 4 are further highlighted in Figure 5 by disparity contours comparing predicted profiles using n = 3, 5, and 10 gray gases. The disparity maps show the difference in prediction of local temperature and local radiative heating between simulations employing a different number of gray gases, calculated from the local

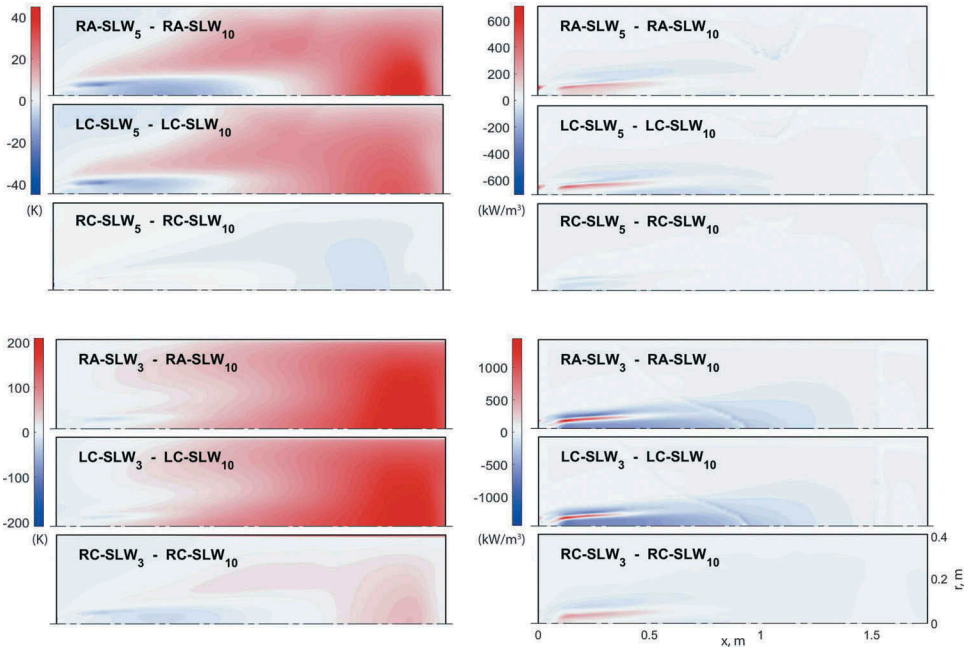

Figure 5. Disparity contours for temperature (left) and radiative heating (right) comparing the 3- and 5-gray-gas predictions to the corresponding 10-gray-gas predictions.

data of Figure 4. Figure 5 reveals that in the case of the RA-SLW and LC-SLW approaches the largest effect of reducing the number of gray gases on the predicted thermal structure of the flame is observed downstream, while the largest effect on flux divergence is observed near the inlet where significant thermal gradients are present. In the case of the RC-SLW approach, however, only very small differences in the predicted temperature fields are observed for n = 10, 5, and 3 gray gases. Similar observations may be made relative to the local radiative heating. The magnitude of the predicted local radiative heating changes quite significantly for the RA-SLW and LC-SLW models as n is reduced from 10 to 5, with differences in Q as high as 700 kW/m^3 (both higher and lower)

Table 2. Computational expense and normalized average and maximum difference data relative to the n = 10 simulation for each of the gas spectral property models.

		Time/Iter.	Temp. Diff.*		Rad. Heat. Diff.*	
Model	n	(s)	Max	Avg	Max	Avg
WSGG	1	0.2	–	–	–	–
RA-SLW	10	2.0	–	–	–	–
	5	1.2	4.1%	1.0%	36.7%	0.16%
	3	0.7	20.8%	7.5%	74.7%	0.58%
LC-SLW	10	2.1	–	–	–	–
	5	1.1	2.9%	0.9%	20.3%	0.12%
	3	0.6	19.2%	7.7%	58.1%	0.48%
RC-SLW	10	2.9	–	–	–	–
	5	1.6	0.8%	0.2%	4.0%	0.04%
	3	1.0	16.2%	1.2%	31.4%	0.24%

*Relative to 10-gray-gas predictions.

observed. By contrast, the predicted radiative heating for the RC-SLW model is nearly independent of the number of gray gases for $3 < n < 10$. It may be concluded that the predictions employing the RC-SLW model are much less dependent on the number of gray gases used than the RA-SLW and LC-SLW models. Indeed, the results show that the RC-SLW model yields accurate predictions for this case with as few as $n = 3$ gray gases. This is quite remarkable, with the conclusion that the RC-SLW model holds promise for very accurate radiative transfer predictions in comprehensive combustion predictions at a reasonable computational cost in practical scenarios where resolving detailed flame zone behavior is critical.

It is worth mentioning that while each of the 5-gray-gas SLW model predictions produced quantitatively similar results to their corresponding 10-gray-gas counterparts, both the RA-SLW and LC-SLW models required that the energy and discrete-ordinates underrelaxation factors be significantly reduced for $n = 5$ to reach a converged solution. The 3-gray-gas RA-SLW and LC-SLW predictions both required a further reduction of underrelaxation factors to reach a converged solution. For the 3-gray-gas simulations with the RA-SLW and LC-SLW models the predicted scalar fields ceased changing with iterations in the numerical solution, but the residuals oscillated somewhat about levels higher than that experienced in either the $n = 5$ or 10 solutions. By contrast, the RC-SLW model was well-behaved numerically when both 3 and 5 gray gases were used and, notably, without requiring reduction in the under-relaxation factors. This suggests that the RC-SLW model is more robust in the numerical computations than either the RA-SLW or LC-SLW model.

A comparison of computation time among the various radiation property models is relevant. Table 2 compares the average computation time per global iteration for all models (HP Elitedesk 800 G4 with Intel i5-8500 processor at 3.0 GHz, 6 cores), as well as the normalized Average and Maximum Difference in T and Q relative to the 10-gray-gas simulation for the three SLW model variants studied. The table illustrates, as expected, that the Average and Maximum Differences in both temperature and radiative heating increase with a reduction of the number of gray gases. The increases are quite significant for the RA-SLW and LC-SLW models. However, the Differences for the RC-SLW model reflect a much more modest dependence on n, confirming the previous observation that accurate predictions may be achieved with the RC-SLW model using fewer gray gases (with attendant lower computation time).

The computation time shown in Table 2 reveals that when n gray gases are used, the computational expense of the RA-SLW and LC-SLW models is approximately n times than that of the WSGG model, while the RC-SLW model is nominally $1.5n$ times that of the computational expense of the WSGG model. The higher computation cost for the RC-SLW model is an artifact of its numerical implementation in the present study, explained as follows. Construction of the gray gas correlated SLW models is carried out using the direct and inverse ALBDF functions. In the current implementation the ALBDF look-up table is used (Pearson et al. 2014). The direct ALBDF is calculated by interpolation of the look-up table data, and the inverse ALBDF is calculated by inversion of the look-up table. As presently implemented, the ALBDF inversion is approximately six times more computationally expensive than the direct ALBDF calculation. Construction of the RA-SLW and LC-SLW spectral models require only one inversion of the ALBDF per gray gas used in in the radiation calculation. By contrast, the current version of the RC-SLW model, which is based on nodes and weights of Gaussian quadratures, requires two ALBDF

inversions per gray gas. Consequently, the computational cost per gray gas of the RC-SLW model is higher. It is important to note again that it has been theoretically shown that the RC-SLW model is the most accurate version of the SLW correlated models (André et al. 2017). Further, it may be mentioned that the RC-SLW model can quite readily be made more efficient if it is constructed in a similar fashion to the RA-SLW and LC-SLW models, with only one ALBDF inversion. This is possible, but has not been implemented in this work. Finally, a more efficient look-up table for which the computation time for the direct and inverse ALBDF operations are equivalent may be developed and implemented (André et al. 2018), or a more efficient numerical ALBDF inversion algorithm may also be explored. Both of these approaches have the potential to result in a RC-SLW model computational cost per gray gas identical to both the RA-SLW and LC-SLW models.

The data of Figures 4 and 5 and Table 1, and the observations regarding numerical stability of the SLW models noted previously suggest that the RC-SLW model is significantly more robust than either of the other two SLW model variants, with less dependence on model and numerical parameters. Stated more succinctly, while the RC-SLW model as currently implemented requires slightly more computational expense per iteration of the RTE solver than the RA-SLW and LC-SLW models, it exhibits numerically robust and accurate behavior even when only a small number of RTEs are used. Further, there is a possibility of improvement in the computational efficiency of the RC-SLW model, rendering it computationally equivalent per gray gas to the RA-SLW and LC-SLW models. Finally, the predictions shown here suggest that solutions may be achieved using the RC-SLW model with superb accuracy using as few as 3–5 gray gases in the calculations. The increased stability and accuracy of the RC-SLW method show a clear advantage over the RA-SLW and LC-SLW methods in comprehensive combustion simulations, and confirm in this comprehensive combustion setting the theoretical finding that the RC-SLW model is the optimal of all correlated SLW model variants (André et al. 2017).

Conclusions

The Reference Approach SLW, Locally Correlated SLW, and Rank Correlated SLW gas spectral property models have been implemented in Fluent, a comprehensive modeling platform for prediction of turbulent reacting flow. Predictions for these three radiation property models are compared to those using the more rudimentary Domain Based Weighted-Sum-of-Gray-Gases Model. The three SLW model variants yield predictions that are quite similar qualitatively and quantitatively, but which differ significantly from predictions using the WSGG model. Each of the SLW model formulations appears to have strengths. The RA-SLW and LC-SLW model predictions show significantly greater dependence on the number of gray gases employed. The RC-SLW model was found to be the most robust numerically and required the fewest gray gases for accurate solutions.

References

Andersson, K., R. Johansson, F. Johnsson, and B. Leckner. 2008. Radiation intensity of propane-fired oxy-fuel flames: Implications for soot formation. *Energy Fuels* 22:1535–41. doi:10.1021/ef7004942.

André, F., V. P. Solovjov, D. Lemonnier, and B. W. Webb. 2017. Co-monotonic global spectral models of gas radiation in nonuniform media based on arbitrary probability measures. *J. Appl. Math. Model.* 50:741–54. doi:10.1016/j.apm.2017.05.033.

André, F., V. P. Solovjov, B. W. Webb, and D. Lemonnier. 2018. Rank transmutation mapping technique for the FSK and SLW models. Proceedings of Eurotherm 110, 6th International Symposium on Computational Thermal Radiation in Participating Media, Cascais, Portugal, April 11-13.

Coppalle, A., and P. Vervisch. 1983. The total emissivity of high-temperature flames. *Combust. Flame* 49:101–08. doi:10.1016/0010-2180(83)90154-2.

Darbandi, M., M. B. Barezban, and G. E. Schneider. 2018. Evaluating the ability of SLW model in numerical simulation of radiative turbulent reacting flow in industrial application. Proc. 5th Joint US-European Fluids Eng. Conf., Montreal, Quebec, July 15-20.

Denison, M. K., and B. W. Webb. 1993. A spectral line-based weighted-sum-of-gray-bases model for arbitrary RTE solvers. *ASME J. Heat Transfer* 115:1004–12. doi:10.1115/1.2911354.

Denison, M. K., and B. W. Webb. 1995a. The spectral line-based weighted-sum-of-gray-gases model in non-isothermal non-homogeneous media. *ASME J. Heat Transfer* 117:359–65. doi:10.1115/1.2822530.

Denison, M. K., and B. W. Webb. 1995b. The spectral-line weighted-sum-of-gray-gases model for H_2O/CO_2 mixtures. *ASME J. Heat Transfer* 117:788–98. doi:10.1115/1.2822652.

Edwards, D. K., and R. Matavosian. 1984. Scaling rules for total absorptivity and emissivity of gases. *ASME J. Heat Transfer* 106:684–89. doi:10.1115/1.3246739.

Garten, B. 2015. Detailed radiation modeling of a particle-oxidation flame. *Int. J. Therm. Sci.* 87:68–84. doi:10.1016/j.ijthermalsci.2014.07.022.

Krishnamoorthy, G., M. Sami, S. Orsino, A. Perera, M. Shahnam, and E. D. Huckaby. 2010. Radiation modeling in oxy-fuel combustion scenarios. *Int. J. Comp. Fluid Dyn.* 24:69–82. doi:10.1080/10618562.2010.485567.

Nguen, P. D., A. Danda, M. Embouazza, M. Gazdallah, P. Evrards, and V. Feldheim. 2012. Application of the spectral line-based weighted-sum-of-gray-gases model (SLWSGG) to the calculation of radiative heat transfer in steel reheating furnaces firing on low heating value gases. *J. Phys.: Conf. Ser.* 369:012008.

Patankar, S. V. 1980. *Numerical heat transfer and fluid flow*. Washington, DC: Hemisphere.

Pearson, J. T., B. W. Webb, V. P. Solovjov, and J. Ma. 2014. Efficient representation of the absorption line blackbody distribution function for H_2O, CO_2, and CO at variable temperature, mole fraction, and total pressure. *J. Quant. Spectr. Rad Transfer* 138:82–96. doi:10.1016/j.jqsrt.2014.01.019.

Rebola, A., and J. L. T. Azevedo. 2015. Modelling pulverized coal combustion using air and O2+recirculated flue gas as oxidant. *Appl. Therm. Eng.* 83:1–7. doi:10.1016/j.applthermaleng.2015.03.008.

Smith, T. F., Z. F. Shen, and J. N. Friedman. 1982. Evaluation of coefficients for the weighted sum of gray gases model. *ASME J. Heat Transfer* 104:602–08. doi:10.1115/1.3245174.

Solovjov, V. P., F. André, D. Lemonnier, and B. W. Webb. 2016. "The generalized SLW model," Eurotherm105: Computational thermal radiation in participating media V, *J. Phys.: Conf. Ser.* 012022 (676):1–36.

Solovjov, V. P., F. André, D. Lemonnier, and B. W. Webb. 2017. The rank correlated SLW model of gas radiation in non-uniform media. *J. Quant. Spectr. Rad. Transfer* 197:26–44. doi:10.1016/j.jqsrt.2017.01.034.

Solovjov, V. P., and B. W. Webb. 2001. An efficient method for modeling radiative transfer in multicomponent gas mixtures with soot. *ASME J. Heat Transfer* 123:450–57. doi:10.1115/1.1350824.

Solovjov, V. P., B. W. Webb, and F. André. 2018. Radiative properties of gases. In *Handbook of thermal science and engineering*, ed. F. A. Kulacki, Vol. 2, 1069–142. New York: Springer.

Solovjov, V. P., B. W. Webb, F. André, and D. Lemonnier. 2019. The locally correlated SLW model of gas radiation in non-uniform media. Proc. 9th Int'l. Symp. Rad. Transfer, Athens, Greece: Begell House, June 3-7.

Webb, B. W., J. Ma, J. T. Pearson, and V. P. Solovjov. 2018. SLW modeling of radiation transfer in comprehensive combustion predictions. *Comb. Sci. Tech.* 190:1392–408. doi:10.1080/00102202.2018.1452123.